Atomic-scale diffusion mechanisms via intermediate species

Ant Ural,* P. B. Griffin, and J. D. Plummer
Department of Electrical Engineering, Stanford University, Stanford, California 94305
(Received 30 January 2001; published 19 March 2002)

We theoretically investigate the relationship between impurity diffusion profiles and the underlying atomic-scale diffusion mechanisms that occur via intermediate species in elemental semiconductors. We focus particularly on diffusion regimes characterized by short versus long diffusion times and low versus high transport capacities. Based on analytic derivations and numerical simulations, we show that, in the absence of any external point defect perturbation, there is usually no unique correspondence between a microscopic diffusion mechanism and a macroscopic impurity diffusion profile. Complementary experiments have to be performed to gain more conclusive information about the microscopic diffusion mechanisms. Examples of these experiments are perturbing the point defect concentrations from equilibrium by thermal oxidation and nitridation, particularly in the short-time diffusion regime, and studying the growth or shrinkage of stacking faults and dislocation loops. Finally, a wide range of impurity diffusion phenomena result from the presence of intermediate species, and can be analytically derived or numerically computed starting from the same set of diffusion equations.

DOI: 10.1103/PhysRevB.65.134303 PACS number(s): 66.30.Dn, 66.30.Jt, 61.72.Ji

I. INTRODUCTION

Substitutional impurity atoms in elemental semiconductors like silicon diffuse by interacting with the native point defects, namely, vacancies (V) and self-interstitials (I), present in the lattice.[1–3] In most cases, intermediate species formed as a result of these interactions are responsible for the overall macroscopic migration of the impurity. However, signs of diffusion via an intermediate species are invisible unless either the diffusion time is short or the concentration and diffusivity of the impurity are high.

Recently, the interest in intermediate diffusion has been revived for two reasons. First, self-diffusion experiments using newly available isotopically enriched Si structures yielded the values of the transport capacities of I and V.[4] Historically, these values have been extracted from diffusion experiments of metals such as Au, Zn, and Pt.[2,5,6] Therefore, a thorough understanding of intermediate diffusion effects is necessary in order to compare point defect properties obtained from self- and metal diffusion experiments.[7] Secondly, recent advances in ultra-low-energy ion-implantation technology have made it possible to fabricate high concentration shallow doping profiles in Si, which are governed by intermediate diffusion effects during annealing even at relatively low temperatures. Therefore, a fundamental understanding of intermediate diffusion has become crucial for advances in semiconductor device fabrication technology.

Some cases of intermediate diffusion effects have been studied previously. The ''kink and tail'' observed in high concentration phosphorus diffusion in silicon[1–3] is a well-known technologically important example. Other well-studied examples are the fast metal diffusers such as Au, Zn, and Pt in Si.[2,5,6] Furthermore, experimental evidence for the intermediate diffusion mechanism of boron in silicon has been obtained at short diffusion times.[8,9]

In this paper, we theoretically study intermediate diffusion in an elemental semiconductor such as Si. The framework presented here is fairly general, and is applicable to any material where an intermediate species determines the overall migration of an impurity. First, we present a general formulation of intermediate diffusion. Then, we define short versus long-time diffusion regimes, and derive analytic solutions for long diffusion times. We also define low versus high impurity transport capacity, and present numerical simulations of in- and out-diffusion in the long-time, high transport capacity limit. Finally, we conclude with a discussion of short-time diffusion. We address the following questions about intermediate diffusion.

(1) What are the different diffusion regimes and the relationship between them?

(2) In which diffusion regimes are the signs of intermediate diffusion visible in macroscopic impurity profiles?

(3) When the signs of intermediate diffusion are visible, is it possible to determine the atomic-scale diffusion mechanism(s) from the experimentally measured diffusion profiles?

We show that, in most cases, it is impossible to derive microscopic diffusion mechanisms from macroscopic diffusion profiles unless complementary experimental information is available. For example, the growth or shrinkage of stacking faults and dislocation loops has been frequently used in the literature to determine whether a particular diffusion process increases or decreases point defect concentrations.[2,3,10] Furthermore, the similarity between the growth kinetics of oxidation induced I-type stacking faults (OSF) and the kinetics of oxidation enhanced diffusion (OED) has lead to the conclusion that thermal oxidation perturbs the point defect concentrations by injecting self-interstitials into the substrate, as first suggested by Hu.[11] As a result, thermal oxidation and nitridation experiments have also been used frequently to obtain information about microscopic diffusion mechanisms.[1–4,12,13]

II. GENERAL FORMULATION OF INTERMEDIATE DIFFUSION

In the following discussion, we assume that impurity diffusion occurs only by intermediate species; in other words, we ignore any direct substitutional exchange contribution to

the overall diffusivity. We also assume that the semiconductor material is under intrinsic carrier conditions; in other words, the Fermi level is at its intrinsic value even in the presence of the impurity. Shifts in the Fermi level cause concentration dependent diffusivity, and introduce electric field induced diffusion of charged defects, which we ignore in this paper. Our conclusions about intrinsic intermediate diffusion can easily be extended to cases where extrinsic effects are important.

To start with, the interaction between a substitutional impurity A and native point defects (I and V) is *completely* specified by the following set of reaction equations:

$$I+A_S \Leftrightarrow AI, \tag{1}$$

$$A_S \Leftrightarrow AI+V, \tag{2}$$

$$V+A_S \Leftrightarrow AV, \tag{3}$$

$$A_S \Leftrightarrow AV+I, \tag{4}$$

$$I+V \Leftrightarrow \varnothing, \tag{5}$$

where A_S denotes impurity A in its substitutional form, and AI and AV are the intermediate species whose migration determines the I and V components of A diffusion, respectively. For example, AI could be an impurity-interstitial pair, an interstitial impurity, or a self-interstitial. $\varnothing$ in reaction Eq. (5) denotes a substitutional host atom. The first two reactions above represent the I component of A diffusion; Eq. (1) is widely known as the kick-out (KO) reaction and Eq. (2) as the dissociative or Frank-Turnbull (FT) reaction. In general, both KO and FT reactions could be responsible for the generation and recombination of AI. The third and fourth reactions, which we refer to as $R3$ and $R4$, respectively, represent the V component of A diffusion. Equation (5), which we denote by IV, modifies the concentrations of I and V available for reactions (1)–(4).

If we take into account all of the five reaction equations (1)–(5), the diffusion of impurity A as a function of time t and position x in one dimension is completely described by the following five coupled partial differential equations (PDE's) with the appropriate boundary conditions specific to the particular problem:

$$\begin{aligned}\frac{\partial C_{A_S}}{\partial t} &= (k_{1r}C_{AI}-k_{1f}C_{A_S}C_I)+(k_{2r}C_{AI}C_V-k_{2f}C_{A_S}) \\ &\quad +(k_{3r}C_{AV}-k_{3f}C_{A_S}C_V)+(k_{4r}C_{AV}C_I-k_{4f}C_{A_S}) \\ &\equiv \left(\frac{\partial C_{A_S}}{\partial t}\right)_1+\left(\frac{\partial C_{A_S}}{\partial t}\right)_2+\left(\frac{\partial C_{A_S}}{\partial t}\right)_3+\left(\frac{\partial C_{A_S}}{\partial t}\right)_4,\end{aligned} \tag{6}$$

$$\frac{\partial C_{AI}}{\partial t} = D_{AI}\frac{\partial^2 C_{AI}}{\partial x^2}-\left(\frac{\partial C_{A_S}}{\partial t}\right)_1-\left(\frac{\partial C_{A_S}}{\partial t}\right)_2, \tag{7}$$

$$\frac{\partial C_{AV}}{\partial t} = D_{AV}\frac{\partial^2 C_{AV}}{\partial x^2}-\left(\frac{\partial C_{A_S}}{\partial t}\right)_3-\left(\frac{\partial C_{A_S}}{\partial t}\right)_4, \tag{8}$$

$$\frac{\partial C_I}{\partial t} = D_I\frac{\partial^2 C_I}{\partial x^2}+\left(\frac{\partial C_{A_S}}{\partial t}\right)_1-\left(\frac{\partial C_{A_S}}{\partial t}\right)_4 -k_5(C_IC_V-C_I^{\mathrm{eq}}C_V^{\mathrm{eq}}), \tag{9}$$

$$\frac{\partial C_V}{\partial t} = D_V\frac{\partial^2 C_V}{\partial x^2}-\left(\frac{\partial C_{A_S}}{\partial t}\right)_2+\left(\frac{\partial C_{A_S}}{\partial t}\right)_3 -k_5(C_IC_V-C_I^{\mathrm{eq}}C_V^{\mathrm{eq}}). \tag{10}$$

In Eqs. (6)–(10), the constants k_{nf} and k_{nr} are the forward and reverse reaction rates, respectively, of Eqs. (1)–(4) where n denotes the number of the reaction equation. In Eqs. (9) and (10), k_5 is the IV recombination rate constant of Eq. (5). C's and D's are the concentrations and diffusivities, respectively, of the species in their subscripts.

III. THE DEFINITION OF SHORT-TIME vs LONG-TIME DIFFUSION

In the short-time and long-time diffusion regimes, Eqs. (6)–(10) can be simplified to give analytic solutions. First, we define the generation rate, the recombination rate, and the migration length of the intermediate species AI and AV. Assuming that KO and FT reactions occur in parallel as statistically independent events (in other words, the defect concentrations are so dilute that there is no interaction between them), the generation and recombination rates for the intermediate species AI are given, respectively, by

$$g_{AI}=k_{1f}C_I+k_{2f} \quad \text{and} \quad r_{AI}=k_{1r}+k_{2r}C_V. \tag{11}$$

Similarly, the generation and recombination rates for AV resulting from reactions $R3$ and $R4$ are, respectively,

$$g_{AV}=k_{3f}C_V+k_{4f} \quad \text{and} \quad r_{AV}=k_{3r}+k_{4r}C_I. \tag{12}$$

The mean migration length of the intermediate species AX ($X=I$ or V) before it recombines to become substitutional is[8]

$$\lambda_{AX}=\sqrt{D_{AX}/r_{AX}}, \tag{13}$$

where D_{AX} is the diffusivity of AX. The forward and reverse reaction rates in Eqs. (11) and (12) are constants at a given temperature. Similarly, under equilibrium point-defect conditions, C_I and C_V are also constants. On the other hand, under nonequilibrium conditions, where C_I and C_V are perturbed from their equilibrium values, Eqs. (11)–(13) become position and time dependent since C_I and C_V are position dependent. The generation rate, the recombination rate, and the migration length that occur under nonequilibrium conditions can be expressed in terms of the equilibrium values of the same quantities as

$$g_{AI}=g_{AI}^{\mathrm{eq}}\left(\gamma_{\mathrm{KO}}\frac{C_I}{C_I^{\mathrm{eq}}}+\gamma_{\mathrm{FT}}\right), \tag{14}$$

$$r_{AI}=r_{AI}^{\mathrm{eq}}\left(\gamma_{\mathrm{KO}}+\gamma_{\mathrm{FT}}\frac{C_V}{C_V^{\mathrm{eq}}}\right), \tag{15a}$$

$$\lambda_{AI}=\lambda_{AI}^{\mathrm{eq}}\left(\gamma_{\mathrm{KO}}+\gamma_{\mathrm{FT}}\frac{C_V}{C_V^{\mathrm{eq}}}\right)^{-1/2}, \tag{15b}$$

$$g_{AV}=g_{AV}^{\mathrm{eq}}\left(\gamma_{R3}\frac{C_V}{C_V^{\mathrm{eq}}}+\gamma_{R4}\right), \tag{16}$$

$$r_{AV}=r_{AV}^{\mathrm{eq}}\left(\gamma_{R3}+\gamma_{R4}\frac{C_I}{C_I^{\mathrm{eq}}}\right), \tag{17a}$$

$$\lambda_{AV}=\lambda_{AV}^{\mathrm{eq}}\left(\gamma_{R3}+\gamma_{R4}\frac{C_I}{C_I^{\mathrm{eq}}}\right)^{-1/2}, \tag{17b}$$

where γ_{KO} and γ_{FT} are the fractional contributions of KO and FT reactions, respectively, to the formation of *AI* under equilibrium point defect conditions. From Eq. (11), we get $\gamma_{\mathrm{KO}}=(k_{1f}C_I^{\mathrm{eq}})/(k_{1f}C_I^{\mathrm{eq}}+k_{2f})=k_{1r}/(k_{1r}+k_{2r}C_V^{\mathrm{eq}})$. Similarly, γ_{R3} and γ_{R4} are the fractional contributions of the $R3$ and $R4$ reactions, respectively, to the formation of *AV* under equilibrium point defect conditions. By definition, $\gamma_{\mathrm{KO}}+\gamma_{\mathrm{FT}}=1$ and $\gamma_{R3}+\gamma_{R4}=1$. The superscript "eq" denotes equilibrium conditions. The generation rate ratio $g_{AX}/g_{AX}^{\mathrm{eq}}$ and the migration length ratio $\lambda_{AX}/\lambda_{AX}^{\mathrm{eq}}$ that occurs under nonequilibrium point defect conditions for each of the reactions (1)–(4) in the absence of the other three are listed in the first and second columns of Table I, respectively. Table I shows that the generation rate and migration length ratio of each possible reaction change in a uniquely different way under nonequilibrium conditions.

The short-time diffusion regime occurs when $g_{AX}t\ll 1$, but $r_{AX}t\gg 1$; in other words, when the diffusion time is short compared to the lifetime of the substitutional impurity, but long compared to the lifetime of the mobile intermediate species. (For the impurities we are considering, the concentration of the substitutional form is much greater than that of the intermediate form, which means that $r_{AX}\gg g_{AX}$, and the short-time diffusion conditions can be satisfied.) Physically, this means that, in the short-time regime, the mean number of migration events of the intermediate species is much less than 1. In the long-time regime, on the other hand, $g_{AX}t, r_{AX}t\gg 1$, which is satisfied when Eqs. (1)–(5) have fast forward and reverse reaction rates and are at chemical quasiequilibrium. On the average, the intermediate species experiences many migration events.

As a simple example, let us consider the transient evolution of A_S and *AI* by the KO mechanism only. For the present discussion, assume that all species are position independent, and that $C_I=C_I^{\mathrm{eq}}$ at all times. Using Eq. (11) under these assumptions, Eqs. (6) and (7) become

$$\frac{\partial C_{A_S}}{\partial t}=r_{AI}C_{AI}-g_{AI}C_{A_S},$$

$$\frac{\partial C_{AI}}{\partial t}=-r_{AI}C_{AI}+g_{AI}C_{A_S}. \tag{18}$$

The solution of Eqs. (18) is given by

$$C_{A_S}(t)=a+b\exp[-(r_{AI}+g_{AI})t],$$

$$C_{AI}(t)=a\frac{g_{AI}}{r_{AI}}-b\exp[-(r_{AI}+g_{AI})t], \tag{19}$$

where a and b are constants to be determined from the boundary conditions. Equations (19) show that if $(r_{AI}+g_{AI})t\gg 1$, A_S and *AI* are at steady-state (chemical quasiequilibrium). This would be satisfied for fast reaction rates and/or long diffusion times. As illustrated by this simple example, quasiequilibrium is characterized in general by $g_{AX}t$, $r_{AX}t\gg 1$.

IV. ANALYTIC SOLUTIONS FOR LONG-TIME DIFFUSION

In the long-time diffusion regime, let us reduce Eqs. (6)–(10) to a single PDE for the substitutional impurity A_S. Adding Eqs. (6)–(8), we get

$$\frac{\partial}{\partial t}(C_{A_S}+C_{AI}+C_{AV})=D_{AI}\frac{\partial^2 C_{AI}}{\partial x^2}+D_{AV}\frac{\partial^2 C_{AV}}{\partial x^2}. \tag{20}$$

Next, we need to write $\partial^2 C_{AX}/\partial x^2$, where $X=I$ or V, in terms of C_{A_S}. Under equilibrium point-defect conditions (i.e., $C_I=C_I^{\mathrm{eq}}$ and $C_V=C_V^{\mathrm{eq}}$), when A_S and *AX* reach steady state, they satisfy the chemical quasiequilibrium conditions for each of the reaction Eqs. (1)–(4):

$$\frac{C_{AI}}{C_{A_S}}=\left(\frac{C_{AI}}{C_{A_S}}\right)^{\mathrm{eq}}=\frac{k_{1f}C_I^{\mathrm{eq}}}{k_{1r}}, \tag{21a}$$

$$\frac{C_{AI}}{C_{A_S}}=\left(\frac{C_{AI}}{C_{A_S}}\right)^{\mathrm{eq}}=\frac{k_{2f}}{k_{2r}C_V^{\mathrm{eq}}}, \tag{21b}$$

$$\frac{C_{AV}}{C_{A_S}}=\left(\frac{C_{AV}}{C_{A_S}}\right)^{\mathrm{eq}}=\frac{k_{3f}C_V^{\mathrm{eq}}}{k_{3r}} \tag{21c}$$

$$\frac{C_{AV}}{C_{A_S}}=\left(\frac{C_{AV}}{C_{A_S}}\right)^{\mathrm{eq}}=\frac{k_{4f}}{k_{4r}C_I^{\mathrm{eq}}}. \tag{21d}$$

From Eqs. (21a) and (21b), we get a relationship between the reactions rates of KO and FT; from Eqs. (21c) and (21d), we get a similar relationship for the $R3$ and $R4$ reactions:

$$\frac{k_{1f}C_I^{\mathrm{eq}}}{k_{1r}}=\frac{k_{2f}}{k_{2r}C_V^{\mathrm{eq}}}\ \text{ and }\ \frac{k_{3f}C_V^{\mathrm{eq}}}{k_{3r}}=\frac{k_{4f}}{k_{4r}C_I^{\mathrm{eq}}}, \tag{22}$$

from which it also follows that

$$C_I^{\mathrm{eq}}C_V^{\mathrm{eq}}=\left(\frac{k_{2f}}{k_{2r}}\right)\left(\frac{k_{1r}}{k_{1f}}\right)=\left(\frac{k_{4f}}{k_{4r}}\right)\left(\frac{k_{3r}}{k_{3f}}\right). \tag{23}$$

Substituting Eqs. (21), and assuming that the concentration of the migrating species is much less than that of the substitutional impurity (i.e., $C_{AX}\ll C_{A_S}$), Eq. (20) becomes

TABLE I. The intermediate species generation rate ratio g_{AX}/g_{AX}^{eq}, the intermediate species migration length ratio $\lambda_{AX}/\lambda_{AX}^{eq}$, and the effective impurity diffusivity ratio D_A/D_A^{eq} that occur under nonequilibrium point defect conditions, and f_{AI} for each of the possible atomic-scale diffusion reactions (1)–(4). For each case, we assume that the other three reactions are negligible. The superscript ''eq'' denotes parameter values under equilibrium point defect conditions. Note that g_{AX}/g_{AX}^{eq} and $\lambda_{AX}/\lambda_{AX}^{eq}$ change in a uniquely different way under nonequilibrium conditions for each reaction.

	Generation rate ratio g_{AX}/g_{AX}^{eq}	Migration length ratio $\lambda_{AX}/\lambda_{AX}^{eq}$	Diffusivity ratio D_A/D_A^{eq}	f_{AI}
(1) $I+A_s \Leftrightarrow AI$	C_I/C_I^{eq}	1	C_I/C_I^{eq}	1
(2) $A_s \Leftrightarrow AI+V$	1	$\sqrt{C_V^{eq}/C_V}$	C_V^{eq}/C_V	1
(3) $V+A_s \Leftrightarrow AV$	C_V/C_V^{eq}	1	C_V/C_V^{eq}	0
(4) $A_s \Leftrightarrow AV+I$	1	$\sqrt{C_I^{eq}/C_I}$	C_I^{eq}/C_I	0

$$\frac{\partial C_{A_S}}{\partial t} = D_A \frac{\partial^2 C_{A_S}}{\partial x^2}, \tag{24}$$

with a constant effective impurity diffusivity D_A given by

$$D_A \equiv D_A^{eq} = D_{AI}\left(\frac{C_{AI}}{C_{A_S}}\right)^{eq} + D_{AV}\left(\frac{C_{AV}}{C_{A_S}}\right)^{eq}, \tag{25}$$

where $(C_{AX}/C_{A_S})^{eq}$ with $X=I$ or V is a constant. Using Eq. (25), the X fraction of A diffusion under equilibrium conditions can be defined as

$$f_{AX} = \frac{D_{AX}(C_{AX}/C_{A_S})^{eq}}{D_A^{eq}}. \tag{26}$$

If only the KO or FT reaction is dominant, $f_{AI}=1$ and $f_{AV}=0$; on the other hand, if only the $R3$ or $R4$ reaction is dominant, $f_{AI}=0$ and $f_{AV}=1$. This is summarized in the fourth column of Table I.

If the IV recombination reaction [Eq. (5)] is also at chemical quasiequilibrium, we get

$$C_I C_V = C_I^{eq} C_V^{eq}. \tag{27}$$

Equation (27) is obviously satisfied under equilibrium point-defect conditions $C_I = C_I^{eq}$ and $C_V = C_V^{eq}$. When point defects are perturbed from equilibrium, Eq. (27) means that the product of the I and V concentrations remains constant, although their individual concentrations may be different from their equilibrium values. Under these conditions, Eq. (24) becomes

$$\frac{\partial C_{A_S}}{\partial t} = \sum_{X=I,V} D_{AX}\left(\frac{C_{AX}}{C_{A_S}}\right)^{eq} \times \left(C_X^{\dagger}\frac{\partial^2 C_{AX}}{\partial x^2} + 2\frac{\partial C_X{}^{\dagger}}{\partial x}\frac{\partial C_{A_S}}{\partial x} + C_{A_S}\frac{\partial^2 C_X{}^{\dagger}}{\partial x^2}\right), \tag{28}$$

where $C_X{}^{\dagger} = C_X/C_X^{eq}$. Under equilibrium I and V conditions, Eq. (28) reduces to Eq. (24) with a constant equilibrium impurity diffusivity given by Eq. (25). Furthermore, if I and V are perturbed from equilibrium in a position-independent manner, Eq. (24) with a constant effective impurity diffusivity D_A such that

$$\frac{D_A}{D_A^{eq}} = f_{AI}\frac{C_I}{C_I^{eq}} + f_{AV}\frac{C_V}{C_V^{eq}} \tag{29}$$

describes diffusion. This is the diffusivity ratio that is frequently cited and generally used for the analysis of thermal oxidation and nitridation experiments in silicon.[1,12,13] Equation (29) shows that it is possible to differentiate between the I and V components of impurity diffusion by perturbing the point defects at long times, but not between the individual mechanisms that make up these components.

There may be situations where the point defects do not satisfy Eq. (27), but A_S and AX are at steady state. This could happen, for example, if IV recombination is much slower than reactions (1)–(4), and only one reaction mechanism is dominant for each intermediate species. Under these circumstances, I and V cannot interact and Eq. (27) does not hold true. However, the steady-state condition still holds true. In other words,

$$C_{AX} = g_{AX} C_{A_S}/r_{AX}. \tag{30}$$

Using Eq. (30), the equivalent of Eq. (28) is

$$\frac{\partial C_{A_S}}{\partial t} = \frac{\partial}{\partial x}\left(D_A \frac{\partial}{\partial x} C_{A_S}\right), \tag{31}$$

where

$$D_A(x,t) \equiv D_{AI}\frac{g_{AI}(x,t)}{r_{AI}(x,t)} + D_{AV}\frac{g_{AV}(x,t)}{r_{AV}(x,t)}, \tag{32}$$

and $g_{AX}(x,t)$ and $r_{AX}(x,t)$ are given by Eqs. (11) and (12). In general, Eq. (32) cannot be simplified further if C_I and C_V are perturbed from equilibrium in a position-dependent manner. However, if the perturbation is such that C_I and C_V are position independent, Eq. (32) simplifies to, using Eq. (26),

$$\frac{D_A}{D_A^{eq}} = f_{AI}\left(\frac{k_{1f}C_I + k_{2f}}{k_{1r} + k_{2r}C_V}\right)\left(\frac{k_{1r} + k_{2r}C_V^{eq}}{k_{1f}C_I^{eq} + k_{2f}}\right) + f_{AV}\left(\frac{k_{3f}C_V + k_{4f}}{k_{3r} + k_{4r}C_I}\right)\left(\frac{k_{3r} + k_{4r}C_I^{eq}}{k_{3f}C_V^{eq} + k_{4f}}\right). \tag{33}$$

The diffusivity ratio in Eq. (33) is a constant. As listed in the third column of Table I, Eq. (33) reduces to a simple expression if only one of the reaction Eqs. (1)–(4) is dominant. This is obtained by setting the forward and reverse reaction rates for the other three reactions to zero. Under equilibrium I and V conditions, Eqs. (31) and (32) reduce to Eqs. (24) and (25).

V. THE DEFINITION OF LOW vs HIGH TRANSPORT CAPACITY

Even when I and V are not perturbed by external forces, they may still be at nonequilibrium as a consequence of Eqs. (1)–(5), provided that the total transport capacity of the impurity is on the order of or greater than those of the native point defects. The transport capacity of the X mechanism mediated diffusion of impurity A is defined as the product $D_{AX}C_{AX}^{\rm eq}$ where $C_{AX}^{\rm eq}=(C_{AX}/C_{A_S})^{\rm eq}C_{A_S}$. It follows that the maximum value that this transport capacity can have is $D_{AX}C_{AX}^{\rm eq,sol}$, where $C_{AX}^{\rm eq,sol}=(C_{AX}/C_{A_S})^{\rm eq}C_{A_S}^{\rm sol}$, and $C_{A_S}^{\rm sol}$ is the solubility of impurity A in the host lattice. The total transport capacity of A defined as the sum $\Sigma_{X=I,V}D_{AX}C_{AX}^{\rm eq}$. Although the total transport capacity of A is a function of C_{A_S}, the transport capacities of I and V, $D_IC_I^{\rm eq}$ and $D_VC_V^{\rm eq}$, respectively, are constants at a given temperature. Thus, transport effects can begin to dominate the shape of impurity profiles at high concentrations.

When $\Sigma_{X=I,V}D_{AX}C_{AX}^{\rm eq}\ll D_IC_I^{\rm eq}$, $D_VC_V^{\rm eq}$, Eqs. (24) and (25) describe the diffusion of the impurity for long-times, and intermediate diffusion effects are invisible. In this low transport capacity limit, it is impossible to distinguish between the KO, FT, $R3$, and $R4$ reactions, since all of them reduce to Eqs. (24) and (25).

When the total impurity transport capacity is on the order of or greater than $D_IC_I^{\rm eq}$ and $D_VC_V^{\rm eq}$, on the other hand, C_I and C_V are perturbed from equilibrium even in the absence of any external perturbing forces. In this high transport capacity limit, Eqs. (28) and (31) describe the diffusion of the impurity at long times, and the presence of intermediate diffusion is evident from the shape of the diffusion profile. In contrast, a direct exchange mechanism would still be described by Eqs. (24) and (25) even if the impurity has a high transport capacity, since there is no interaction with the native point defects. If KO is the only dominant diffusion mechanism, and we are in the very high transport capacity limit such that $\Sigma_{X=I,V}D_{AX}C_{AX}^{\rm eq}\gg D_IC_I^{\rm eq}$, $D_VC_V^{\rm eq}$ and $C_{AI}(x,t)\cong C_{AI}^{\rm eq,sol}$, Eq. (9) becomes

$$\frac{\partial C_I}{\partial t}=D_I\frac{\partial^2 C_I}{\partial x^2}+\frac{\partial C_{A_S}}{\partial t}. \tag{34}$$

Assuming chemical quasiequilibrium [Eq. (21a)], we get $C_I=C_I^{\rm eq}C_{A_S}^{\rm sol}/C_{A_S}$. Substituting this expression for C_I into Eq. (34), and using $C_{A_S}^2\gg C_I^{\rm eq}C_{A_S}^{\rm sol}$, we arrive at an expression having the form of Eq. (31) with

$$D_A^{\rm KO}(x,t)=\frac{D_IC_I^{\rm eq}C_{A_S}^{\rm sol}}{C_{A_S}^2(x,t)}. \tag{35}$$

This is the frequently cited inverse-concentration-squared dependent diffusivity.[2,5,6] We can see from Eq. (35) that the diffusion coefficient of the impurity is determined by the transport capacity of self-interstitials. Using a similar argument, if FT is the only dominant mechanism, we get

$$D_A^{\rm FT}=\frac{D_VC_V^{\rm eq}}{C_{A_S}^{\rm sol}}, \tag{36}$$

which is a constant. If both KO and FT mechanisms exist, but $R3$ and $R4$ are insignificant (in other words, AI is the only intermediate species), the effective diffusivity is the sum of Eqs. (35) and (36). It is worth emphasizing that this expression is valid only if the other two reactions do not contribute to diffusion, the transport capacity of the impurity is high, and KO and FT reactions are at quasiequilibrium. With these assumptions $C_{A_S}\approx C_{A_S}^{\rm sol}$, so Eqs. (35) and (36) describe the profiles after very long diffusion times when there is not much net impurity motion taking place. On the other hand, if only the $R3$ and $R4$ reactions determine impurity diffusion (in other words, AV is the only intermediate species),

$$D_A=\frac{D_VC_V^{\rm eq}C_{A_S}^{\rm sol}}{C_{A_S}^2}+\frac{D_IC_I^{\rm eq}}{C_{A_S}^{\rm sol}}, \tag{37}$$

and the vacancy term is concentration dependent. If both AI and AV intermediate species are responsible for diffusion, simple expressions similar to Eqs. (35)–(37) cannot be obtained.

As seen in Eqs. (35)–(37), the transport capacities of I and V, which can be determined by studying the interstitial and vacancy components of self-diffusion,[4] play an important role in the diffusion of impurities with high transport capacities. The study of self-diffusion in a host lattice is closely tied to the study of impurity diffusion.

VI. NUMERICAL SIMULATION OF LONG-TIME, HIGH TRANSPORT CAPACITY DIFFUSION

In this section, we study the relationship between microscopic diffusion mechanisms and macroscopic impurity diffusion profiles in the long-time, high transport capacity regime by performing in- and out-diffusion simulations using ALAMODE,[14] a numerical partial differential equation solver optimized for diffusion problems. In these simulations, we meet the long-time diffusion criteria by assigning Eqs. (1)–(5) fast forward and reverse reaction rates.

We have solved subsets of reaction Eqs. (6)–(10) numerically subject to in- and out-diffusion initial and boundary conditions. In particular, the in-diffusion boundary conditions we have used are

$$C_I(x=0,t)=C_I(x=1,t)=C_I^{\rm eq}, \tag{38a}$$

$$C_V(x=0,t)=C_V(x=1,t)=C_V^{\rm eq}, \tag{38b}$$

$$C_{AX}(x=0,t)=C_{AX}(x=1,t)=C_{AX}^{\rm eq,sol}, \tag{38c}$$

$$C_{A_S}(x=0,t)=C_{A_S}(x=1,t)=C_{A_S}^{\rm sol}\{1-\exp[-(g_{AI}+g_{AV})t]\}, \tag{38d}$$

where x is the normalized depth, t is time, and other variables have been defined previously. Equation (38d) is obtained by solving Eq. (6) at $x=0$ and 1. Furthermore, we have used the following initial conditions for in-diffusion:

$$C_{A_S}(x,t=0)=C_{A_S}^{\mathrm{sol}}\times 10^{-10}$$

$$C_{AX}(x,t=0)=C_{AX}^{\mathrm{eq,sol}}\times 10^{-10}, \tag{39a}$$

$$C_I(x,t=0)=C_I^{\mathrm{eq}}$$

$$C_V(x,t=0)=C_V^{\mathrm{eq}}. \tag{39b}$$

The out-diffusion initial and boundary conditions for C_I and C_V are the same as those for in-diffusion. For the impurity concentrations during out-diffusion, we have used

$$C_{A_S}(x=0,t)=C_{A_S}(x=1,t)=C_{A_S}^{\mathrm{sol}}\times 10^{-4}, \tag{40a}$$

$$C_{AX}(x=0,t)=C_{AX}(x=1,t)=C_{AX}^{\mathrm{eq,sol}}\times 10^{-4}, \tag{40b}$$

$$C_{A_S}(x,t=0)=C_{A_S}^{\mathrm{sol}} \quad \text{and} \quad C_{AX}(x,t=0)=C_{AX}^{\mathrm{eq,sol}}. \tag{40c}$$

Using these initial and boundary conditions, first, let us consider the diffusion mechanisms via *AI*, which correspond to the *I* component of impurity diffusion (i.e., $f_{AI}=1$). Figures 1(a) and 1(b) show the time evolution of in- and out-diffusion profiles, respectively, of impurity *A* when KO [Eq. (1)] is the only dominant diffusion mechanism. All other reactions, including IV recombination, are assumed to be negligible. During in-diffusion, the center of the sample initially has no impurity, and Eq. (1) is driven in the reverse direction, creating excess *I* above equilibrium. On the other hand, during out-diffusion, the center of the sample is saturated with the impurity to begin with, and Eq. (1) is driven in the forward direction, depleting *I* from the center. Since *I* and *V* do not interact, *V* remains at equilibrium at all times regardless of what happens to *I*. As a consequence, the impurity diffusion profile is sensitive to $D_I C_I^{\mathrm{eq}}$, but not to $D_V C_V^{\mathrm{eq}}$, during both in- and out-diffusion.

Figures 2(a) and 2(b) show the time evolution of in-and out-diffusion profiles, respectively, when FT [Eq. (2)] is the only dominant diffusion mechanism. As in Figs. 1(a) and 1(b), no interaction between *I* and *V* exists. During in diffusion, Eq. (2) is driven in the reverse direction, depleting *V*. On the other hand, during out diffusion Eq. (2) is driven in the forward direction, creating excess *V*. Since *I* and *V* do not interact, *I* remains at equilibrium at all times, and, as a consequence, the impurity diffusion profile is sensitive to $D_V C_V^{\mathrm{eq}}$, but not to $D_I C_I^{\mathrm{eq}}$.

Let us now consider the diffusion mechanisms via *AV*, which correspond to the *V* component of impurity diffusion (i.e., $f_{AI}=0$). If $R3$ is the only dominant mechanism, there is *V* supersaturation during in-diffusion and *V* undersaturation during out-diffusion, and the impurity profile is sensitive

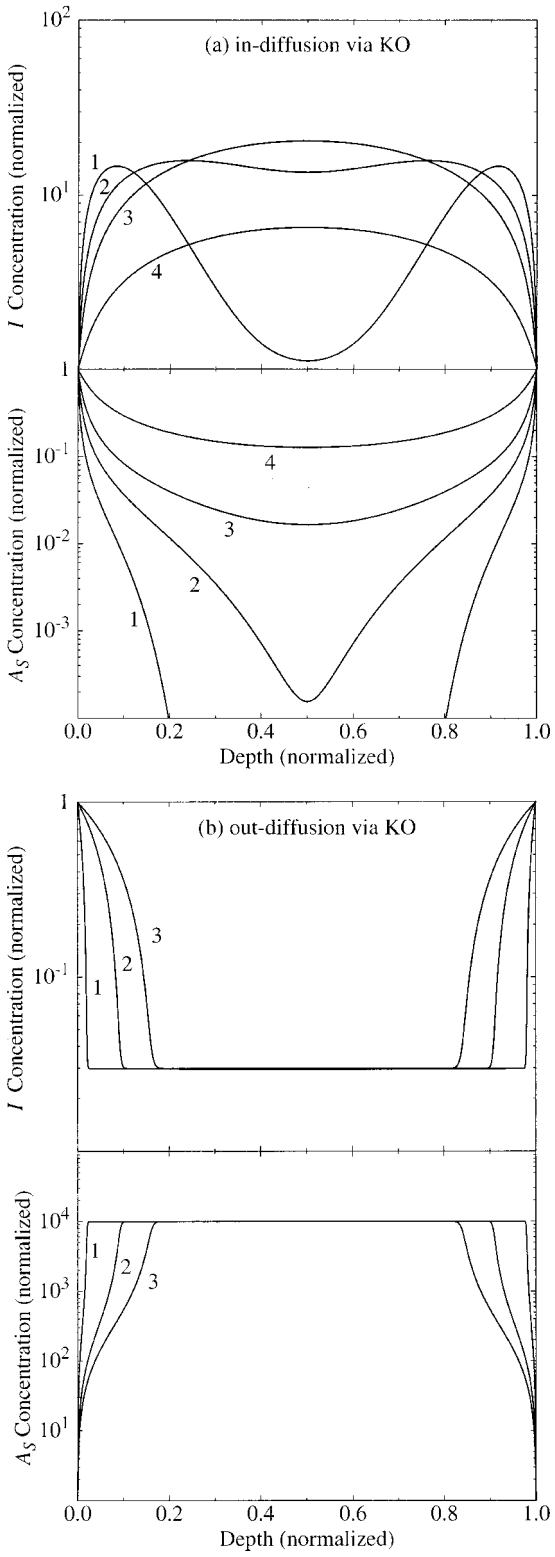

FIG. 1. The concentration of impurity *A* in substitutional sites C_{A_S} normalized to its solubility (bottom) and the self-interstitial concentration C_I normalized to its equilibrium value (top) in the host lattice as a function of normalized depth in a hypothetical sample. (a) In-diffusion and (b) out-diffusion profiles resulting from the KO mechanism alone. The curves are labeled by numbers in the order of increasing diffusion time. The normalized *V* concentration, which is not shown, is equal to unity.

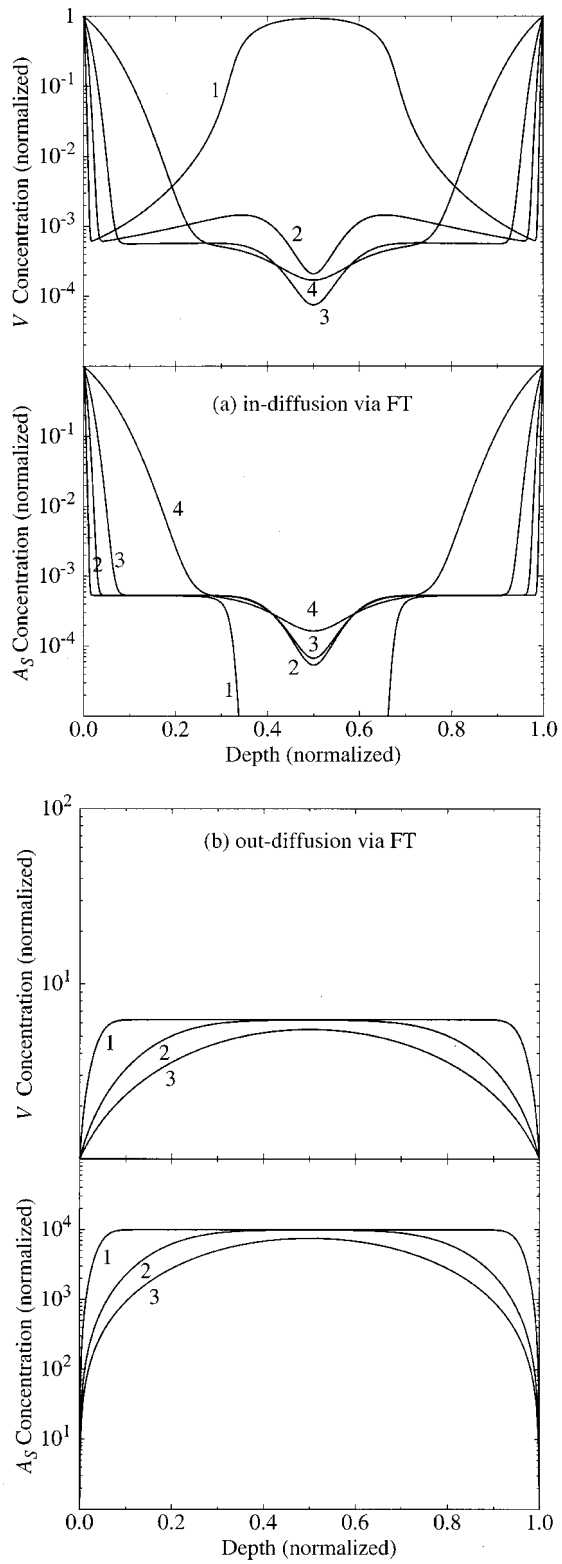

FIG. 2. C_{A_S} normalized to its solubility (bottom) and the vacancy concentration C_V normalized to its equilibrium value (top) in the host lattice as a function of normalized depth in a hypothetical sample. (a) In-diffusion and (b) out-diffusion profiles resulting from the FT mechanism alone. The curves are labeled by numbers in the order of increasing diffusion time. The normalized *I* concentration, which is not shown, is equal to unity.

only to $D_V C_V^{eq}$. If *R*4 is the only dominant reaction, on the other hand, *I* undersaturation during in-diffusion and *I* supersaturation during out-diffusion results, and the impurity profile is sensitive only to $D_I C_I^{eq}$. In the special case $D_{AV}(C_{AV}/C_{A_s})^{eq} = D_{AI}(C_{AI}/C_{A_s})^{eq}$, $(C_{AV}/C_{A_s})^{eq} = (C_{AI}/C_{A_s})^{eq}$, $D_I C_I^{eq} = D_V C_V^{eq}$, and $C_I^{eq} = C_V^{eq}$, *R*3 and KO and FT and *R*4 reactions produce identical impurity profiles. In others words, replacing *AI* by *AV*, *I* by *V*, and *V* by *I*, diffusion profiles via *AI* and *AV* are completely symmetric in this special case. The fact that KO and *R*3 are equivalent under these circumstances has already been pointed out by Shaw.[15]

In- and out-diffusion simulations in Figs. 3(a) and 3(b), respectively, show that KO-IV, FT-IV, KO-FT, and KO-FT-IV reaction combinations give identical diffusion profiles for given values of $C_{A_s}^{sol}$, $D_{AI}(C_{AI}/C_{A_s})^{eq}$, $D_I C_I^{eq}$, $D_V C_V^{eq}$, $(C_{AI}/C_{A_s})^{eq}$, C_I^{eq}, and C_V^{eq}. In Figs. 3(a) and 3(b), we have assumed that all the reactions present in each case have fast forward and reverse reaction rates (long-time regime) so that they are at chemical quasiequilibrium [Eqs. (21a), (21b), and (27)]. Under these conditions, Eq. (27) is satisfied at all positions, and the *V* profile is always the mirror image of the *I* profile on a log scale. As a result, the impurity diffusion profile is sensitive to both $D_I C_I^{eq}$ and $D_V C_V^{eq}$. Based on Figs. 3(a) and 3(b), we conclude that it is impossible to distinguish between the KO and FT mechanisms *in the presence of IV recombination at long diffusion times*. This has already been pointed out by Frank *et al.*[2] We can see this conclusion from Table I as follows. If in-diffusion occurs by the KO reaction, the generation rate of *AI* increases, but its migration length stays the same; on the other hand, if it occurs by the FT reaction, the generation rate of *AI* stays the same, but its migration length increases. At long diffusion times, the overall diffusivity, which is proportional to $g_{AI}\lambda_{AI}^2$, is the same for both reactions if Eq. (27) holds. Although what takes place microscopically is quite different in the case of KO or FT, the net macroscopic effect on diffusion is identical.

Another point to note is that the in-diffusion profiles generated by KO-IV, FT-IV, KO-FT, or KO-FT-IV reaction combinations [Fig. 3(a)] resemble closely those generated by the KO reaction alone [Fig. 1(a)], but are quite different from those generated by the FT reaction alone [Fig. 2(a)]. This is a consequence of the fact that the *I* supersaturation required for A_S and *AI* to reach steady-state is much less than the required *V* undersaturation [compare Figs. 1(a) and 2(a)]. Once A_S and *AI* reach equilibrium at an *I* supersaturation similar in magnitude to that of the KO reaction alone, there is no driving force to deplete *V* further. The out-diffusion profiles generated by KO-IV, FT-IV, KO-FT, or KO-FT-IV reaction combinations, on the other hand, resemble closely those generated by the FT reaction alone [Fig. 2(b)], but are quite different from those generated by the KO reaction alone [Fig. 1(b)]. This is a consequence of the fact that the *V* supersaturation required for A_S and *AI* to reach steady state is much less than the required *I* undersaturation.

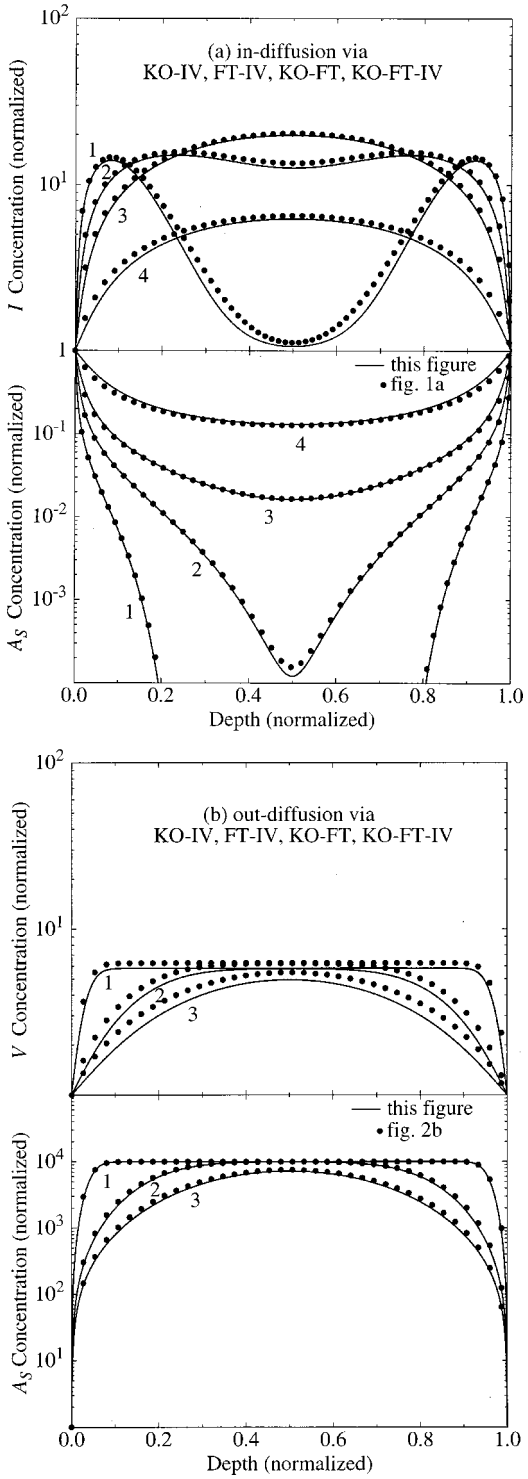

FIG. 3. C_{A_S} normalized to its solubility (bottom), and C_I or C_V normalized to its equilibrium value (top) as a function of normalized depth in a hypothetical sample. (a) In-diffusion and (b) out-diffusion profiles resulting from KO-IV, FT-IV, KO-FT, or KO-FT-IV reaction combinations. These profiles are indistinguishable and appear as a single solid line for each time snapshot. The curves are labeled by numbers in the order of increasing diffusion time. The normalized V concentration is always the mirror image of the normalized I concentration, and vice versa. For comparison, the KO-only profiles for in-diffusion [Fig. 1(a)], and FT-only profiles for out-diffusion [Fig. 2(b)] are shown as symbols.

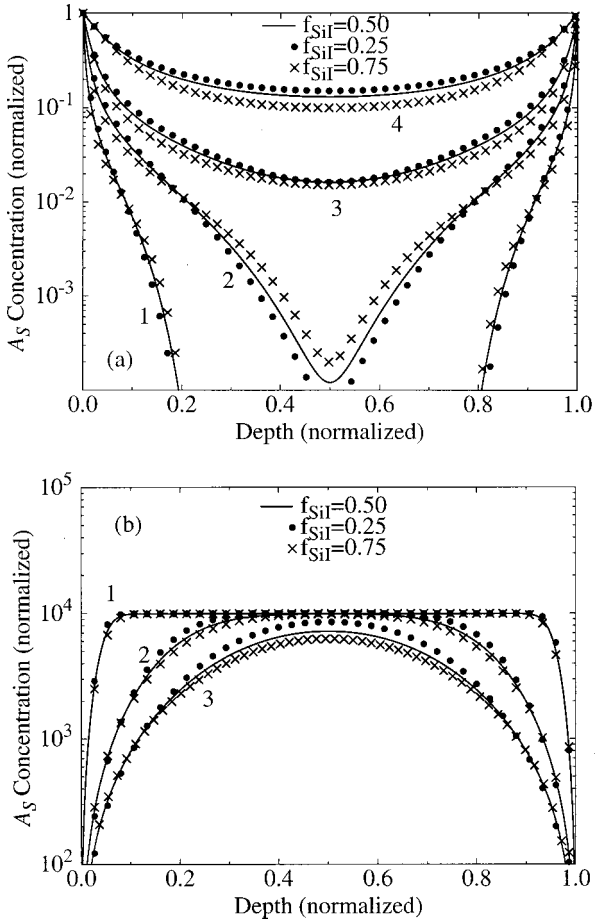

FIG. 4. The effect of the I fraction of self-diffusion f_{SiI} on the diffusion of impurity A when the I fraction of A diffusion f_{AI} is zero. (a) In-diffusion and (b) out-diffusion profiles resulting from $R3$-IV, $R4$-IV, $R3$-$R4$, or $R3$-$R4$-IV reaction combinations. These profiles are indistinguishable and appear as a single solid line for each time snapshot. The curves are labeled by numbers in the order of increasing diffusion time.

In- and out-diffusion simulations under conditions similar to those in Figs. 3(a) and 3(b) show that $R3$-IV, $R4$-IV, $R3$-$R4$, and $R3$-$R4$-IV reaction combinations, which occur via the intermediate species AV, give identical profiles for given values of $C_{A_S}^{\mathrm{sol}}$, $D_{AV}(C_{AV}/C_{A_s})^{\mathrm{eq}}$, $D_I C_I^{\mathrm{eq}}$, $D_V C_V^{\mathrm{eq}}$, $(C_{AV}/C_{A_s})^{\mathrm{eq}}$, C_I^{eq}, and C_V^{eq}. Based on this, we conclude that it is impossible to distinguish between reactions $R3$ and $R4$ in the presence of IV recombination at long diffusion times. Figures 4(a) and 4(b) show time series of in- and out-diffusion profiles, respectively, occurring by $R3$-IV, $R4$-IV, $R3$-$R4$, or $R3$-$R4$-IV reactions. As mentioned above, all of these reaction combinations result in the same impurity profile. The effect of the I fraction of self-diffusion f_{SiI} on the profiles is shown explicitly.

Finally, let us consider the situation when both I and V components of impurity diffusion exist (i.e., $0<f_{AI}<1$). In particular, let us consider the following 14 subsets of reaction Eqs. (1)–(5): KO-FT-$R3$-$R4$-IV, KO-FT-$R3$-IV, KO-FT-$R4$-IV, KO-$R3$-$R4$-IV, FT-$R3$-$R4$-IV, KO-FT-$R3$-$R4$, KO-$R3$-IV, KO-$R4$-IV, FT-$R3$-IV,

FT-$R4$-IV, KO-FT-$R3$, KO-FT-$R4$, KO-$R3$-$R4$, and FT-$R3$-$R4$. If all of the reactions present in each case are individually at quasi-equilibrium, it is not possible to distinguish between these 14 reaction combinations for given values of the simulation parameters and f_{AI}. Furthermore, if $f_{AI}>0.5$, there is always an I supersaturation and V undersaturation for in-diffusion, and vice versa for out-diffusion. The opposite is true if $f_{AI}<0.5$. If $f_{AI}=0.5$, both I and V are at equilibrium, because perturbations in opposite directions exactly cancel out. In this special case, we go back to equilibrium diffusion described by Eqs. (24) and (25). The effects of intermediate diffusion via AI and AV exactly cancel each other out. Figures 5(a) and 5(b) illustrate the effect of f_{AI} on in- and out-diffusion, respectively. As we have mentioned previously, the V profile in each case is the mirror image of the I profile, and vice versa. In Figs. 5(a) and 5(b), we have taken $(C_{AV}/C_{A_s})^{\rm eq}=(C_{AI}/C_{A_s})^{\rm eq}$, $D_I C_I^{\rm eq}=D_V C_V^{\rm eq}$, and $C_I^{\rm eq}=C_V^{\rm eq}$ for symmetry. In this special case, the impurity profiles for $f_{AI}=0.25$ and 0.75, and $f_{AI}=0$ and 1 are equivalent. From Figs. 4 and 5, we see that both f_{AI} and f_{SiI} affect the diffusion profiles, once again illustrating that self-diffusion is closely tied to impurity diffusion in a lattice.

We have seen that although a single microscopic diffusion mechanism directly interacts with only one point defect, the interaction between self-interstitials and vacancies causes an ambiguity on the macroscopic scale. Indeed, using reasonable diffusion parameters, macroscopic experimental diffusion data can be fit more than a unique combination of microscopic diffusion mechanisms.[16] As we have pointed out in the introduction, the only way of determining microscopic diffusion mechanisms is by obtaining additional experimental information such as the growth or shrinkage of stacking faults and dislocation loops of a certain type. As an example, Marioton *et al.* have previously shown that enhanced and retarded diffusion phenomena in silicon can be explained based only on the FT and $R3$ reactions.[17] They have also shown, however, that these two reactions alone cannot quantitatively explain the growth of oxidation induced I-type stacking faults. As a result, they have concluded that reactions involving I must also be present.

VII. SHORT-TIME DIFFUSION

The generation rate g_{AX} and migration length λ_{AX} of the intermediate species AX can be extracted independently from experimental diffusion profiles in the short-time diffusion regime if there is only one intermediate species present. Let us first consider the short-time diffusion regime in the low impurity transport capacity limit. As we have seen before, this is characterized mathematically by $g_{AX}t\ll 1$, $r_{AX}t\gg 1$, $C_I=C_I^{\rm eq}$, and $C_V=C_V^{\rm eq}$. Under these conditions, the solution of Eqs. (6)–(8) subject to the in-diffusion initial and boundary conditions [Eqs. (38) and (39)] is given by

$$C_{A_s}(x,t)=C_{A_s}^{\rm sol}[g_{AI}t\exp(-x/\lambda_{AI})+g_{AV}t\exp(-x/\lambda_{AV})]. \tag{41}$$

Equation (41) can be obtained by writing Eqs. (6)–(8) in terms of the generation rates g_{AI} and g_{AV} and migration

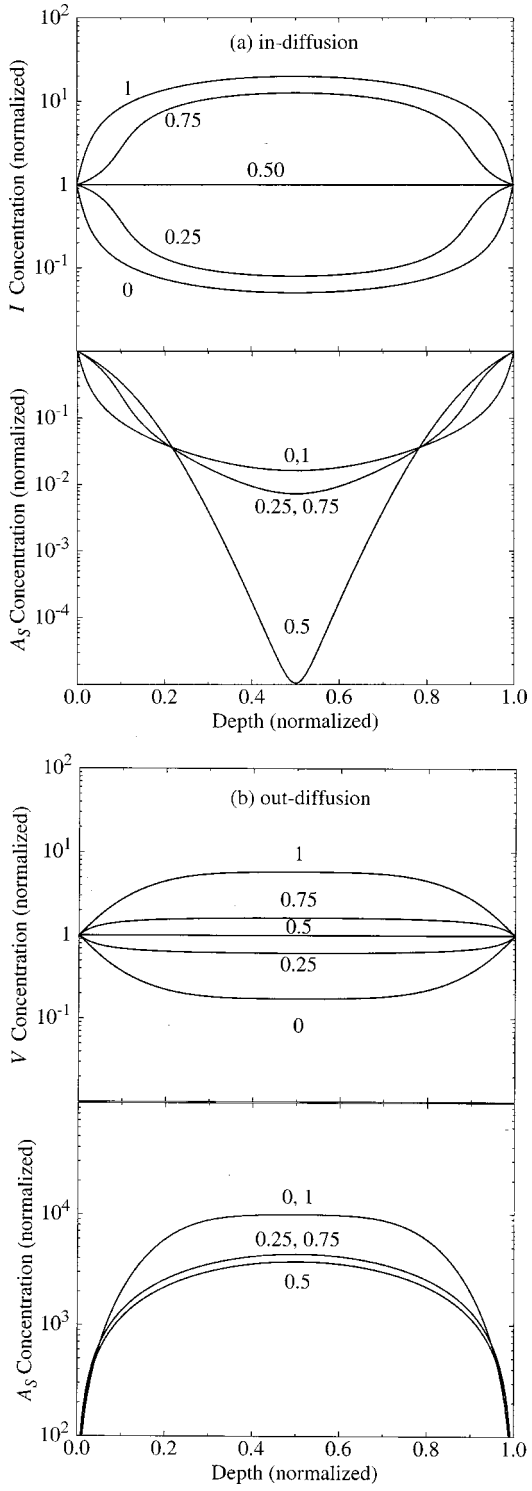

FIG. 5. C_{A_S} normalized to its solubility (bottom), and C_I or C_V normalized to its equilibrium value (top) as a function of normalized depth in a hypothetical sample. (a) In-diffusion and (b) out-diffusion profiles when there is both an I and V component of impurity diffusion (i.e., $0<f_{AI}<1$). Each line is labeled by its value of f_{AI}. The profiles obtained for the possible reaction combinations listed in the text that give a particular value of f_{AI} are indistinguishable and appear as a single line. The normalized V concentration is the mirror image of the normalized I concentration, and vice versa. Note that when $f_{AI}=0.5$, C_I and C_V are exactly at equilibrium.

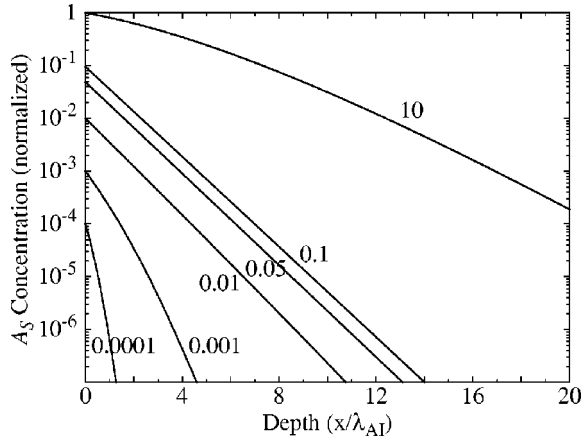

FIG. 6. In-diffusion profiles of *A* normalized to the solubility as a function of normalized depth in a hypothetical sample showing the different diffusion regimes. Only one intermediate species *AI* mediates diffusion, and the curves are labeled by their values of $g_{AI}t$. The simulation parameters are given in the text. The exponential diffusion regime occurs for $g_{AI}t=0.01$, 0.05, and 0.1.

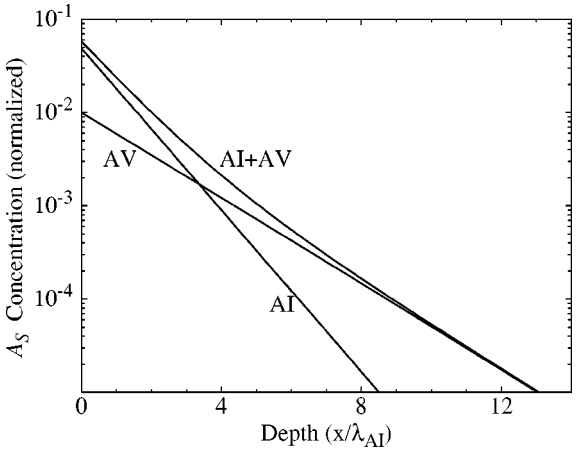

FIG. 7. In-diffusion simulations of impurity *A* via both *AI* and *AV* for $t=500$ s, which corresponds to $g_{AI}t=0.05$ and $g_{AV}t=0.01$. The simulation parameters are given in the text. The individual exponential components of *AI* and *AV* as well as their sum is shown. In this particular case, the sum is no longer an exponential.

lengths λ_{AI} and λ_{AV} defined previously in Eqs. (11)–(13). Extending the derivation of Lever and Morehead[18] to the case of two intermediate species, we arrive at Eq. (41). If only one intermediate species is present (either *AI* or *AV*), then Eq. (41) simplifies to a pure exponential with its slope yielding the migration length, and its *y* intercept the generation rate of the intermediate species. When there is no external perturbation of the point defects, and the impurity has a low transport capacity $g_{AI}=g_{AI}^{\rm eq}$, $\lambda_{AI}=\lambda_{AI}^{\rm eq}$, $g_{AV}=g_{AV}^{\rm eq}$, and $\lambda_{AV}=\lambda_{AV}^{\rm eq}$. Under these conditions, it is impossible to distinguish between the KO, FT, *R*3, *R*4, KO-FT, and *R*3-*R*4 reaction combinations in the short-time regime, since all of them result in an exponential profile. However, the presence of two intermediate species (*AI* and *AV*) can be identified even under equilibrium conditions as long as *AI* and *AV* have different generation rates and migration lengths. In this case, the impurity profile is no longer a single exponential, but the sum of two exponentials with different slopes and *y* intercepts. Nevertheless, it is impossible to distinguish between the different reaction combinations which lead to two intermediate species.

Figure 6 shows an in-diffusion simulation of impurity *A* via the intermediate species *AI* in the low transport capacity limit, and under equilibrium point-defect conditions. For this particular simulation, we have chosen $g_{AI}=1\times10^{-4}$ s^{-1}, $r_{AI}=0.1$ s^{-1}, and $\lambda_{AI}=10\ \mu$. Figure 6 shows that at very-short diffusion times such that $g_{AI}t$, $r_{AI}t\ll1$, the diffusion profiles are complementary error function (erfc)-like, as explained in Ref. 18. At short times such that $g_{AI}t\ll1$, but $r_{AI}t\gg1$, the diffusion profiles are exponential as given by the *AI* term in Eq. (41). Note also that the boundary condition implied by Eq. (41), i.e., $C_{A_s}(x=0,t)=C_{A_s}^{\rm sol}(g_{AI}+g_{AV})t$ is exactly the same as that given in Eq. (38d) in the short-time limit $g_{AX}t\ll1$. For longer times such that $g_{AI}t$, $r_{AI}t\gg1$, the diffusion profiles are described by the solution of Eqs. (24) and (25) as illustrated by the $g_{AI}t=10$ curve in Fig. 6. Furthermore, from the slope of the $g_{AI}t=0.05$ profile in Fig. 6, we get $\lambda_{AI}=10\ \mu$, and from the *y* intercept, we get $g_{AI}=1\times10^{-4}$ s^{-1}. These are precisely the values we used in the simulations.

Figure 7 shows an in-diffusion simulation of impurity *A* via both *AI* and *AV* in the low transport capacity limit, and under equilibrium point-defect conditions for $t=500$ s. Also shown are the individual components *AI* and *AV* for the same diffusion time. We have used $g_{AI}=1\times10^{-4}$ s^{-1}, $g_{AV}=0.2\times10^{-4}$ s^{-1}, $r_{AI}=0.1$ s^{-1}, $r_{AV}=0.02$ s^{-1}, $\lambda_{AI}=10\ \mu$, and $\lambda_{AV}=20\ \mu$. This corresponds to $f_{AI}=0.56$. The presence of two migrating species is easily identifiable from the shape of the diffusion profile, but the KO-FT and *R*3-*R*4 reaction pairs cannot be distinguished unless the generation rates and migration lengths for *AI* and *AV* are known.

If C_I and C_V are perturbed from their equilibrium values in a position-independent manner, such as near the surface during oxidation and nitridation of Si, the first two columns of Table I show that the generation rate and migration length for each of the possible reactions (1)–(4) change in a uniquely different way, but still remain independent of time and position. This means that Eq. (41) still applies with g_{AI}, g_{AV}, λ_{AI}, and λ_{AV} given by Eqs. (14), (16), (15b), and (17b), respectively. In other words, the generation rate, the migration length, and as a result, the diffusion profile depend on the values of $\gamma_{\rm KO}$, $\gamma_{\rm FT}$, γ_{R3}, and γ_{R4}. Therefore, by comparing equilibrium and perturbed diffusion profiles, it may be possible to identify the underlying atomic-scale diffusion mechanisms. Figure 8 shows an in-diffusion simulation of impurity *A* when $C_I=4C_I^{\rm eq}$ and $C_V=C_V^{\rm eq}$ with the same equilibrium generation rates and migration lengths as in Fig. 7. We present profiles at $t=500$ s for KO, FT, *R*3, *R*4, KO-FT with $\gamma_{\rm KO}=0.3$, and *R*3-*R*4 with $\gamma_{R3}=0.6$. For the KO-FT reaction combinations, the *y*-intercept changes, whereas for the *R*3-*R*4 reaction combinations, the slope changes.

Cowern *et al.* have experimentally measured boron diffusion in silicon in the short-time regime and extracted values for g_{AI} and λ_{AI} using delta-doped layers grown by MBE.[8]

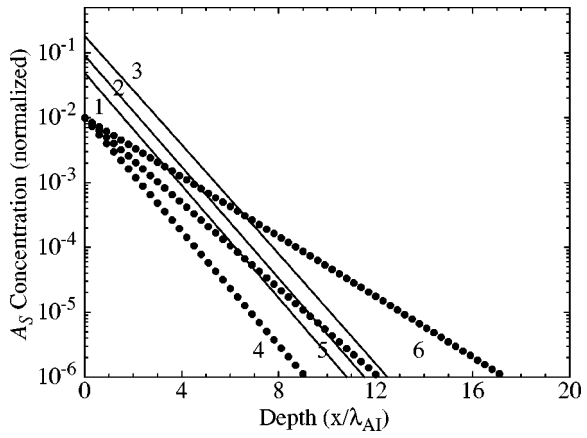

FIG. 8. In-diffusion simulations of impurity A when the point defect concentrations are externally perturbed from equilibrium such that $C_I = 4C_I^{eq}$ and $C_V = C_V^{eq}$. Diffusion profiles are shown at $t = 500$ s, and the equilibrium simulation parameters of Fig. 7 are used. Diffusion via FT (curve 1), KO (curve 3), and KO-FT with $\gamma_{KO} = 0.3$ (curve 2) are shown as solid lines. Changing the value of γ_{KO} moves the y-intercept of curve 2 between curves 1 and 3, but does not change its slope. Diffusion via $R3$ (curve 6), $R4$ (curve 4), and $R3$-$R4$ with $\gamma_{R3} = 0.6$ (curve 5), on the other hand, are shown as symbols. Changing the value of γ_{R3}, moves the slope of curve 5 between those of curves 4 and 6, but does not change the y intercept. If both AI and AV intermediate species are present, the diffusion profile is obtained by adding the solid line with the appropriate γ_{KO} and the symbols with the appropriate γ_{R3}.

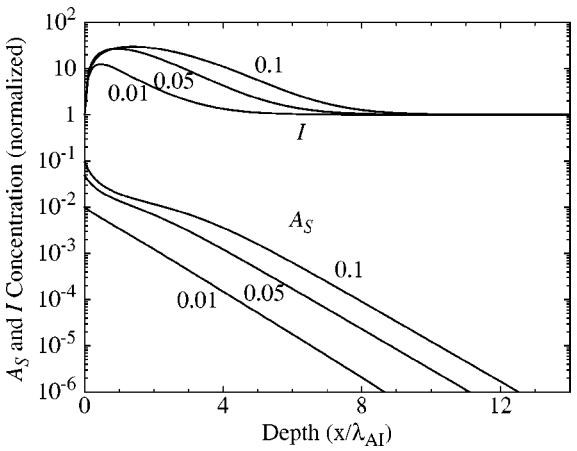

FIG. 9. In-diffusion simulation of impurity A via only the KO reaction using the same parameters as in Fig. 6, except for a six orders of magnitude smaller $D_I C_I^{eq}$. This puts the impurity in the high transport capacity regime, and as a result, C_I is perturbed in a position-dependent manner close to the surface. This perturbation causes the diffusion profiles to deviate from the exponential form observed in Fig. 6. The curves are labeled by their values of $g_{AI}t$.

Extending their derivation[19] for a single intermediate species to the case of two intermediate species, we find that the diffusion of an initial δ-function impurity profile can be described by, to first order in $g_{AX}t$,

$$C_{A_S}(x,t) = [1-(g_{AI}+g_{AV})t]\delta(x) + \frac{g_{AI}t}{2\lambda_{AI}} \times \exp(-|x|/\lambda_{AI}) + \frac{g_{AV}t}{2\lambda_{AV}}\exp(-|x|/\lambda_{AV}). \tag{42}$$

In other words, during the diffusion of an initial δ-function profile, exponential tails with characteristic length λ_{AX} appear on both sides, and the magnitude of these tails increases with time proportional to g_{AX}/λ_{AX}. Equation (42) assumes, as in Eq. (41), that g_{AX} and λ_{AX} are constants. In other words, Eq. (42) is valid either when I and V are at equilibrium, or when they are perturbed in a position-independent manner. Extracting g_{AX} and λ_{AX} under equilibrium and thermal oxidation conditions, Cowern *et al.* have determined experimentally that boron in Si diffuses predominantly by a kick-out mechanism.[9] A similar procedure could identify the diffusion mechanisms of other impurities given that their migration lengths are long enough to be experimentally observed. As Fig. 8 shows, this identification could be much harder if there are multiple intermediate species and mechanisms present.

So far, we have only dealt with the low transport capacity limit. In the high transport capacity limit, the generation rates and migration lengths are no longer constants, and Eqs. (41) and (42) are no longer valid. Figure 9 shows an in-diffusion simulation of impurity A via only the KO reaction with the same parameters as in Fig. 6, except with a six orders of magnitude smaller $D_I C_I^{eq}$. Figure 9 shows that the I concentration is perturbed in a position-dependent manner close to the surface due to the high transport capacity of the impurity. As a result, the diffusion profiles deviate from the exponential form given by Eq. (41). This simple example illustrates that the determination of microscopic diffusion mechanisms becomes more complicated in the high transport capacity limit.

For long diffusion times $g_{AI}t$, $r_{AI}t \gg 1$, only the average impurity diffusivity can be extracted, and separate identification of g_{AX} and λ_{AX} becomes impossible. The relationship between the effective impurity diffusivity D_A, the mean migration length λ_{AX}, and the generation rate g_{AX} is obtained if we use Eq. (13) in Eq. (32) to get

$$D_A = g_{AI}\lambda_{AI}^2 + g_{AV}\lambda_{AV}^2. \tag{43}$$

In Eq. (43), g_{AX} and λ_{AX} become constants if C_I and C_V are position-independent, in which case Eq. (33) can be rewritten as

$$\frac{D_A}{D_A^{eq}} = f_{AI}\frac{g_{AI}\lambda_{AI}^2}{g_{AI}^{eq}(\lambda_{AI}^{eq})^2} + f_{AV}\frac{g_{AV}\lambda_{AV}^2}{g_{AV}^{eq}(\lambda_{AV}^{eq})^2}. \tag{44}$$

Equation (44) shows that if the diffusivity ratio D_A/D_A^{eq} is measured in an experiment where the diffusion time is long, the microscopic information contained separately in g_{AX} and λ_{AX} is lost; it is only the product $g_{AX}\lambda_{AX}^2$ which can be determined.

VIII. CONCLUSIONS

In conclusion, we have made explicit the connections between short versus long-time diffusion, low versus high impurity transport capacity, equilibrium versus perturbed point defect concentrations, and impurity versus self-diffusion. We have emphasized that all these phenomena are special cases of diffusion via intermediate species, and can all be derived starting from the same set of partial differential equations.

Furthermore, using analytic and numerical analysis, we have shown clearly that in the absence of external point-defect perturbation, there is usually no unique correspondence between a microscopic diffusion mechanism and a macroscopic impurity profile. As a result, complementary experimental information, such as the growth or shrinkage of stacking faults and dislocation loops of a given type need to be used to arrive at reliable conclusions. In addition, point defect concentrations can be perturbed from equilibrium in a controlled way by thermal oxidation and nitridation of Si. In the long-time diffusion regime, this makes it possible to differentiate between the I and V components of impurity diffusion, but not between the individual mechanisms that make up these components. In the short-time regime, this perturbation makes it possible to extract the changes in the generation rate and migration length of the intermediate species independently, and determine the dominant atomic-scale diffusion mechanisms. However, this method may not unambiguously reveal the underlying mechanisms if the exponential diffusion profiles are obscured by the high transport capacity of the impurity or the existence of multiple intermediate species.

ACKNOWLEDGMENTS

This work was funded by the Semiconductor Research Corporation.

*Electronic mail: antural@stanfordalumni.org

[1] P. M. Fahey, P. B. Griffin, and J. D. Plummer, Rev. Mod. Phys. **61**, 289 (1989), and references therein.

[2] W. Frank, U. Gösele, H. Mehrer, and A. Seeger, in *Diffusion in Crystalline Solids*, edited by G. E. Murch and A. S. Nowick (Academic, New York, 1984), p. 63, and references therein.

[3] S. M. Hu, Mater. Sci. Eng., R. **13**, 105 (1994), and references therein.

[4] Ant Ural, P. B. Griffin, and J. D. Plummer, Phys. Rev. Lett. **83**, 3454 (1999).

[5] H. Bracht, N. A. Stolwijk, and H. Mehrer, Phys. Rev. B **52**, 16 542 (1995), and references therein.

[6] T. Y. Tan and U. Gösele, Appl. Phys. A: Solids Surf. **37**, 1 (1985); F. Morehead, N. A. Stolwjik, W. Meyberg, and U. Gösele, Appl. Phys. Lett. **42**, 690 (1983).

[7] H. Bracht and E. E. Haller, Phys. Rev. Lett. **85**, 4835 (2000); Ant Ural, P. B. Griffin, and J. D. Plummer, *ibid.* **85**, 4836 (2000).

[8] N. E. B. Cowern, K. T. F. Janssen, G. F. A. van de Walle, and D. J. Gravesteijn, Phys. Rev. Lett. **65**, 2434 (1990).

[9] N. E. B. Cowern, G. F. A. van de Walle, D. J. Gravesteijn, and C. J. Vriezema, Phys. Rev. Lett. **67**, 212 (1991).

[10] U. Gösele and W. Frank, in *Defects in Semiconductors*, edited by J. Narayan and T. Y. Tan (North Holland, New York, 1981), p. 55.

[11] S. M. Hu, J. Appl. Phys. **45**, 1567 (1974).

[12] Ant Ural, Peter B. Griffin, and James D. Plummer, Appl. Phys. Lett. **73**, 1706 (1998).

[13] Ant Ural, Peter B. Griffin, and James D. Plummer, J. Appl. Phys. **85**, 6440 (1999).

[14] ALAMODE computer code provided by D. W. Yergeau, Stanford University.

[15] D. Shaw, Phys. Status Solidi A **86**, 629 (1984).

[16] Ant Ural (unpublished).

[17] B. P. R. Marioton, U. Gösele, and T. Y. Tan, Chemtronics **1**, 156 (1986).

[18] R. F. Lever and F. F. Morehead, J. Appl. Phys. **73**, 1139 (1993).

[19] N. E. B. Cowern and G. F. A. Van de Walle, Mod. Phys. Lett. B **5**, 1555 (1991).